ACCEPTED FOR PUBLICATION IN THE ASTROPHYSICAL JOURNAL
Preprint typeset using LaTeX style emulateapj v. 4/12/04

THE BARYON CONTENT OF DARK MATTER HALOS: EMPIRICAL CONSTRAINTS FROM MG II ABSORBERS

HSIAO-WEN CHEN AND JEREMY L. TINKER
Dept. of Astronomy & Astrophysics and Kavli Institute for Cosmological Physics, University of Chicago, Chicago, IL, 60637, U.S.A.
hchen@oddjob.uchicago.edu

Accepted for Publication in the Astrophysical Journal

ABSTRACT

We study the extent and covering fraction of cool baryons around galaxies of different luminosity and mass, based on a survey of Mg II $\lambda\lambda 2796, 2803$ absorption features near known galaxies. The initial sample consists of 13 galaxy and absorber pairs and 10 galaxies that do not produce Mg II absorption lines to within sensitive upper limits. The redshifts of the galaxy and absorber pairs range from $z = 0.2067$ to 0.892 with a median of $z = 0.3818$. We find that galaxies at larger impact parameters produce on average weaker Mg II absorbers. This anti-correlation is substantially improved when accounting for the intrinsic luminosities of individual galaxies. In addition, there exists a distinct boundary at $\rho = R_{\rm gas}$, beyond which no Mg II absorbers are found. A maximum likelihood analysis shows that the observations are best described by an isothermal density profile and a scaling relation $R_{\rm gas} = 91 \times (L_B/L_{B_*})^{(0.35\pm0.05)}\ h^{-1}$ kpc (or 69 h^{-1} kpc at $W(2796) = 0.3$ Å) with a mean covering factor of $\langle\kappa\rangle = 80-86$ %. Together with the scaling relation between halo mass and galaxy luminosity inferred from halo occupation studies, this scaling of $R_{\rm gas}$ indicates that gas radius is a fixed fraction of the dark matter halo radius. We compare our results with previous studies and discuss the implications of our analysis for constraining the baryon content of galactic halos and for discriminating between competing scenarios for understanding the nature of the extended gas.

Subject headings: cosmology: observations—intergalactic medium—quasars: absorption lines

1. INTRODUCTION

The Mg II $\lambda\lambda 2796, 2803$ doublets are among the absorption features commonly seen in the spectra of distant quasars that are produced by intervening gaseous clouds along the quasar lines of sight. Their rest-frame absorption equivalent width $W(2796)$, ranging from $W(2796) \lesssim 0.3$ Å to $W(2796) > 2$ Å (e.g. Steidel & Sargent 1990; Nestor et al. 2005; Prochter et al. 2006a), is found to represent the underlying gas kinematics (e.g. Petitjean & Bergeron 1990; Churchill et al. 2000). Based on comparisons of the abundance ratios of various associated ions, these Mg II absorption transitions are understood to arise primarily in photo-ionized gas of temperature $T \sim 10^4$ K (Bergeron & Stasínska 1986; Hamann 1997) and neutral hydrogen column density $N(\mathrm{H\,I}) = 10^{18} - 10^{22}$ cm^{-2} (Churchill et al. 2000; Rao et al. 2006). In addition, surveys for galaxies near the observed Mg II absorbers have often uncovered luminous galaxies at projected distances ($\rho \lesssim 50\ h^{-1}$ kpc) and velocity separations ($\Delta v \leq 250$ km s^{-1}) from the absorbers (Bergeron 1986; Lanzetta & Bowen 1990, 1992; Steidel et al. 1994; Zibetti et al. 2005; Nestor et al. 2007; Kacprzak et al. 2007). The relatively large associated $N(\mathrm{H\,I})$ and the small separation between Mg II absorbers and galaxies along common lines of sight indicate that Mg II absorbers may offer a sensitive probe of photo-ionized halo gas around galaxies at redshifts from $z = 0.3$ to $z = 2.3$ in the optical spectral window.

Understanding the physical origin of these Mg II absorbers bears significantly on all efforts to apply their known statistical properties for constraining the baryon content of dark matter halos on different mass scales (Tinker & Chen 2008). Various theoretical models have been developed in the past that describe the nature of the absorbers in the context of gas accretion, including ram pressure stripped gas from accreted satellites (Wang 1993), gravitationally bound cold gas in halo substructures (e.g., Sternberg et al. 2002), and condensed cold clouds in a thermally unstable hot halo (Mo & Miralda-Escude 1996; Maller & Bullock 2004; Chelouche et al. 2007).

Insights to the origin of Mg II absorbers can be obtained from their clustering amplitude on large scales ($\gtrsim 1\,h^{-1}$ Mpc). The clustering of the absorbers is a consequence of dark matter halos in which they are found. Measurements of the galaxy and absorber cross–correlation function offer a means of quantifying the mean halo mass of the absorbers. High-mass halos are expected to be highly clustered, while low mass halos on average have weaker clustering strength. The cross–correlation function of Mg II absorbers and luminous red galaxies (LRGs) have been measured at $\langle z\rangle = 0.6$ by Bouché et al. (2006), who found that Mg II absorbers of $W(2796) > 0.3$ Å cluster strongly with LRGs and that weaker absorbers with $W(2796) = 0.3 - 1.15$ Å on average arise in dark matter halos that are 10 times more massive than those of stronger absorbers with $W(2796) = 2 - 2.85$ Å.

Both the observed clustering amplitude and the inverse correlation between the mean halo mass and absorber strength are difficult to interpret. For example, the frequency distribution function of Mg II absorbers show that there are on average 10 times more $W(2796) = 1$ Å absorbers than those of $W(2796) = 2$ Å (e.g. Nestor et al. 2005; Prochter et al. 2006a) which, when combined with the clustering measurements, implies that the majority of absorbers reside in massive, highly biased halos. At the same time, we expect that observed Mg^+ ions originate primarily in photo-ionized gas of temperature $T \sim 10^4$ K and the halo gas in massive dark matter halos becomes too hot for abundant Mg^+ to survive.

In Tinker & Chen (2008; hereafter TC08), we developed a new technique that adopts the halo occupation framework for understanding the origin of QSO absorption-line systems. Specifically, the technique adopts a model density profile for the Mg^+ ions in individual dark matter halos. The "cold" baryon content of individual dark matter halos, as probed by

the presence of Mg^+, is then constrained through matching the space density and clustering amplitude of dark matter halos with the observed frequency distribution function of Mg II absorbers and their clustering amplitude. Our model allows the possibility that a predominant fraction of the gas in massive halos is shock heated to the virial temperature of the halo and becomes too hot to host abundant Mg II absorbing clouds. Within the hot halo, we further allow the possibility that some dense, cold clouds may penetrate through as seen in high resolution cosmological simulations (Kravtsov 2003). The result of this halo occupation analysis is the probability function $P(W|M_h)$ that characterizes, for each dark matter halo of M_h, the total probability of finding a Mg II absorber of equivalent width W.

The halo occupation analysis shows that observations, including both the Mg II absorber frequency distribution function and their clustering amplitude, demand a rapid transition in the halo gas content at $M_h^{crit} \sim 10^{11.5}\ h^{-1}\,\mathrm{M}_\odot$. Below M_h^{crit}, halos contain predominantly cold gas and therefore contribute significantly to the observed Mg II statistics. Beyond M_h^{crit}, the cold gas fraction is substantially reduced and presumably the halo gas becomes too hot to maintain a large contribution to Mg II absorbers. In order to reproduce the observed overall strong clustering of the absorbers and the inverse correlation between $W(2796)$ and halo mass M_h, roughly 5% of the gas in halos up to $10^{14}\ h^{-1}\,\mathrm{M}_\odot$ is required to be cold. It is understood under our model that *the $W(2796)$ vs. M_h inverse correlation arises mainly as a result of an elevated clustering amplitude of $W(2796) \lesssim 1$ Å absorbers, rather than a suppressed clustering strength of $W(2796) \gtrsim 2$ Å absorbers.* The clustering amplitude of weak absorbers is elevated because of the presence of cold streams in massive hot halos. The amount of cold gas in clusters is small, therefore these halos can only contribute to weak absorbers.

The initial results of our halo occupation analysis demonstrate that combining known statistics of dark matter halos with a simple model for their gas content can already reproduce the statistical properties known for Mg II absorbers. It provides a simple prescription for populating baryons in dark matter halos that can be compared directly to results from numerical simulations and offer insights for understanding the physics of gas accretion in halos of all mass scales. However, some uncertainties remain in the halo occupation analysis.

First, a key parameter that constrains the distribution of Mg^+ ions in individual dark matter halos is their incidence rate, $\kappa(M_h)$, per halo. It specifies the total probability of detecting an absorber in a halo of mass M_h. In the halo occupation analysis of TC08, we find that dark matter halos of $M_h = 10^{11.5\text{–}12.5}\ h^{-1}\,\mathrm{M}_\odot$ on average have 100% incidence rate of Mg^+ ions, $\langle\kappa(M_h)\rangle = 1$, at $R_{\rm gas} \leq R_{200}/3$ for Mg^+ ions and $\langle\kappa(M_h)\rangle = 0$ at larger radii.[1] In halos of lower masses, $\langle\kappa(M_h)\rangle$ declines sharply.

While a 100% incidence rate shows that every dark matter halo hosts a uniform gaseous halo of Mg^+ ions with size $R_{\rm gas}$, the low $\langle\kappa(M_h)\rangle$ is more difficult to interpret because $\langle\kappa(M_h)\rangle$ represents a mean value averaged over all halos of mass M_h. A low $\langle\kappa(M_h)\rangle$ may be a result of only a small fraction of dark matter halos containing extended distributions of Mg^+ ions or a result of a small covering factor of Mg^+ in all halos. In addition, we have assumed in our initial analysis that the gaseous extent is related to halo mass according to $R_{\rm gas} = R_{\rm gas*}\,[M_h/(10^{12}\,h^{-1}\,\mathrm{M}_\odot)]^\beta$, and $R_{\rm gas*} = 50\ h^{-1}$ physical kpc and $\beta = 1/3$. This scaling relation follows the theoretical expectation between virial radius and halo mass, but a higher $R_{\rm gas}$ would naturally lower κ for a fixed frequency distribution function of Mg II absorbers.

Second, the physical origin of the cold clouds probed by the Mg II absorption transitions is ambiguous. While the mass scale at which halo gas is found to experience a transition from a cold-mode dominated state to a hot-mode dominated state agrees well with the expectation of theoretical models established to characterize the gas accretion history in dark matter halos (e.g. Birnboim & Dekel 2003; Kereŝ et al. 2005; Dekel & Birnboim 2006; Birnboim et al. 2007), the observed cold-hot transition can also be interpreted as a declining formation efficiency of cool clouds in a hot halo with increasing halo mass (e.g. Mo & Miralda-Escude 1996; Maller & Bullock 2004). Both of these scenarios predict that halo gas is primarily cold at $M_h \lesssim 10^{11.5}\,h^{-1}\,\mathrm{M}_\odot$. On the other hand, Bouché et al. (2006) have argued that the inverse correlation between $W(2796)$ and clustering amplitude is suggestive of the absorbers arising in non-virialized gas flows, such as starburst winds.

While dense clumps in starburst driven outflows are expected to contribute to some fraction of the observed Mg II absorbers, an important quantity to specify is the significance of this fraction. If a large fraction of Mg II absorbers originate in cold dense clumps in starburst winds, then one must also account for the more complex star formation physics in efforts to apply known Mg II statistics for constraining the gas content of dark matter halos. We defer to § 5.3 for a more detailed discussion of the caveats in interpreting the known properties of Mg II absorbers as evidence to support their origin in starburst winds.

Direct constraints on the covering fraction of Mg II absorbing gas versus halo mass not only help to break the degeneracy between the fraction of dark matter halos containing cold baryons and the extent of cold gas in individual halos, in principle they also serve to discriminate between the starburst wind scenario and gas accretion. Under the starburst wind scenario, superwind driven outflows are expected to proceed over a finite angular span along the minor axis (e.g. Heckman et al. 1990; Veilleux et al. 2005), and result in only partial covering of the halos. In addition, because at a given epoch only some fraction of galaxies are found at starburst or post-starburst stages, we would expect a fraction of dark matter halos to contain extended Mg II absorbing gas due to outflows.

To obtain empirical constraints on the extent and covering fraction of Mg^+ ions around galaxies of different luminosity and mass, we have initiated a survey of Mg II absorbers around known galaxies at small projected distances ($\rho \lesssim 100\,h^{-1}$ kpc) to a background QSO. Accounting the presence or absence of Mg II absorbers for an unbiased sample of galaxies at different impact parameters yields a statistical estimate of the gas covering fraction around field galaxies. A detailed comparison between the absorber strength and galaxy properties further constrains the density profile and extent of the gas. The primary objectives of our study are (1) to improve the uncertainties of our halo occupation analysis by obtaining empirical measurements of $R_{\rm gas}$ and β, and (2) to examine whether starburst driven outflows are the predominant mechanism for producing the observed Mg II absorbers by obtaining an empirical constraint of the gas covering factor

[1] The halo size R_{200} corresponds to the radius, within which the enclosed mean density is $200 \times \bar{\rho}_m$ and $\bar{\rho}_m$ is the background density. It is motivated by estimates of the virial radius both from the spherical collapse model and from N-body simulations that predict $\approx 180 \times \bar{\rho}_m$.

κ. Here we present the initial results of our study.

This paper is organized as follows. In Section 2, we describe the design of our experiment for constraining the extent and covering fraction of Mg^+ ions. In Section 3, we describe the imaging and spectroscopic data available for our experiment. In Section 4, we examine the correlation between Mg II absorption strength and galaxy properties, such as the impact parameter and luminosity. We compare our results with previous studies and discuss the implications of our analysis in Section 5. We adopt a ΛCDM cosmology, $\Omega_M = 0.3$ and $\Omega_\Lambda = 0.7$, with a dimensionless Hubble constant $h = H_0/(100 \text{ km s}^{-1} \text{ Mpc}^{-1})$ throughout the paper.

2. EXPERIMENT DESIGN

Accurate estimates of the extent and covering fraction of Mg^+ ions around galaxies require an unbiased survey of Mg II absorbers in the vicinity of *known* galaxies. Nearly all studies published in the literature to date focus on surveys of galaxies that correspond to known Mg II absorbers (e.g. Bergeron 1986; Lanzetta & Bowen 1990, 1992; Steidel et al. 1994; Zibetti et al. 2007; Kacprzak et al. 2007), with the exception of an on-going study described in Tripp & Bowen (2005). Searching for galaxies that give rise to known Mg II absorbers bears a large uncertainty due to contamination from galaxies that are correlated with the true absorbing galaxies. In addition, these surveys based on known presence of Mg^+ ions do not yield constraints on the incidence of these ions in galactic halos.

We are conducting a survey of Mg II absorbers at the locations of known galaxies close to the line of sight toward a background QSO. We identify galaxies at impact parameters $\rho \leq r_0$. The value of r_0 is selected to allow identifications of galaxies at impact parameters beyond the size of extended Mg II halos, in order to constrain the extent and covering fraction of the gas. At the same time, we require r_0 to be small enough in order to minimize the contamination of galaxies that do not give rise to the absorbers but are merely correlated with the absorbing galaxies through clustering.

To estimate the contamination rate of correlated galaxies as a function of projected distance, we adopt the distribution of dark matter halos identified in cosmological simulations as a guide. We use the $z = 0.5$ output of a 400 h^{-1} co-moving Mpc simulation described in Tinker et al. (2007). First, we identify for each random line of sight dark matter halos that have $M_h \geq 10^{11}\ h^{-1}\,M_\odot$ and are located at $\rho \leq R_{200}/3$ from the sightline. From TC08, we consider these halos likely to host a Mg II absorber along the line of sight. This is also consistent with the results from the halo occupation distribution models of galaxies found in DEEP2 and Sloan Digital Sky Survey from Zheng, Coil, & Zehavi (2007; hereafter ZCZ07). These authors found that the minimum mass of a dark matter halo that on average hosts a galaxy of $\gtrsim 0.1 L_*$ is $\approx 2 \times 10^{11}$ $h^{-1}\,M_\odot$. Next, for each potential Mg II absorber, we search for neighboring halos that are at $|\delta v| \leq 250$ km s^{-1} and projected distance less than ρ from the absorber and may therefore contaminate the search of the true absorber. Finally, we repeat this exercise over 10,000 random lines of sight and calculate the frequency of finding contaminating halos as a function of ρ.

The result of our exercise is presented in Figure 1, where we show the probability of contamination due to correlated galaxies versus impact parameter. The errorbars represent the 68% scatter of the mean from 16 jackknife subsamples. Figure 1 shows that at $\rho > 100\ h^{-1}$ physical kpc there is a $> 30\%$ chance that one would mis-identify a correlated galaxy as the true absorber. Combining the contamination rate estimates with previous search reports that indicate a mean gaseous extent of $\sim 50\ h^{-1}$ physical kpc for luminous galaxies (Bergeron 1986; Lanzetta & Bowen 1990, 1992; Steidel et al. 1994), we carry out our study based on a sample of galaxies that are within $r_0 = 100\ h^{-1}$ kpc from a background QSO.

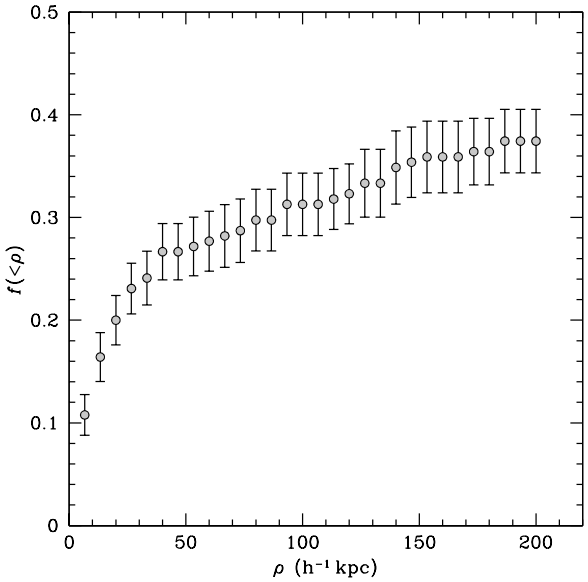

FIG. 1.— The probability of finding more than one galaxy with $|\delta v| \leq 250$ km s^{-1} and at projected distances less than ρ from an absorber. The errorbars represent the 68% scatter that was estimated using a jackknife resampling technique.

3. DATA

To study the extent and covering fraction of Mg^+ ions in galactic halos, it requires survey data of both galaxies and absorbers along common lines of sight toward background quasars. We have selected seven QSO fields for which galaxies data are already available, and echelle spectra of the background QSOs have also been obtained either from our own observations or through the ESO science data archive. We describe available QSO spectra and galaxy data separately in the following sections.

3.1. *Echelle Spectra of QSOs*

Echelle spectroscopic observations of the QSOs, PKS 0122–0021 (z_{QSO} = 1.0765), HE 0226–4110 (z_{QSO} = 0.495), PKS 0349–1438 (z_{QSO} = 0.6163), and PKS 0454–2203 (z_{QSO} = 0.5335) were obtained using the MIKE echelle spectrograph (Bernstein et al. 2003) on the Magellan Clay telescope in 2007 October. The spectrograph contains a blue camera and a red camera, allowing a full wavelength coverage from near-ultraviolet 3350 Å through near-infrared 9400 Å. Depending on the brightness of the QSO, the observations were carried out in a sequence of one to three exposures of duration 600 s to 900 s each. The mean seeing condition over the period of integration was 0.7″. We used a 1″ slit and 2×2 binning during readout, yielding a spectral resolution of FWHM ≈ 13 km s^{-1} at wavelength λ = 4500 Å and ≈ 16 km s^{-1} at λ = 8000 Å. The data

were processed and reduced using the MIKE data reduction software developed by Burles, Prochaska, & Bernstein[2]. Wavelengths were calibrated to a ThAr frame obtained immediately after each exposure and subsequently corrected to vacuum and heliocentric wavelengths. Flux calibration was performed using a sensitivity function derived from observations of the flux standard EG131. The flux calibrated spectra have a mean $S/N > 25$ per resolution element across the entire spectral range.

Echelle spectra of the QSOs, PKS1354+1933 ($z_{\rm QSO}$ = 0.7200), PKS1424−1150 ($z_{\rm QSO}$ = 0.8060), and PKS1622+23 ($z_{\rm QSO}$ = 0.927) were obtained using the Ultraviolet and Visual Echelle Spectrograph (UVES; D'Odorico et al. 2000) on the VLT/UT2 telescope and were retrieved from the ESO data archive. Observations of PKS1354+1933 (program ID 076.A−0860) and PKS1424−1150 (program ID 075.A−0841) were obtained using a 1″ slit and the dichroics #1 B346+R580 and #2 B437+R860 in a sequence of two to three exposures of duration 180s to 300 s each. The data were binned 2×2 during readout. Observations of PKS 1622+23 (program ID 069.A−0371) were obtained using a 1″ slit and the dichroic #1 B346+R580 in a sequence of three exposures of duration 4900 s each. The data were also binned 2×2 during readout. The UVES spectra were processed and calibrated using the standard data reduction pipeline. The combined spectra of the three QSOs cover a spectral range from 3300 Å to 6600 Å, with a pixel scale of 0.035 Å per pixel and $S/N > 10$ per pixel at $\lambda > 3700$ Å. The high S/N and high spectral resolution MIKE and UVES spectra together allow us to search for Mg II absorption features at redshifts $0.2 < z < 2.3$ to a limiting absorption strength $W(2796) = 0.01$ Å along the lines of sight toward the seven background QSOs.

3.2. *The Galaxy Sample*

For the purpose of the study described in § 2, we need to identify a representative sample of galaxies at $\rho \lesssim 100\ h^{-1}$ kpc from the background QSOs. Galaxies in six of the seven QSO fields listed in Table 1 have been observed and analyzed by Chen et al. (1998, 2001a). Specifically, galaxies in the fields around PKS 0122−0021, PKS 0349−1438, and PKS 0454−2203, PKS1354+1933, and PKS1424−1150 were observed as part of the survey program to study the gaseous extent of galaxies based on the presence or absence of corresponding Lyα and C IV absorption features in the spectra of the background QSOs (Lanzetta et al. 1995; Chen et al. 1998, 2001a; Chen et al. 2001b). The authors carried out a redshift survey of galaxies brighter than R = 21.5 mag at angular distances $\theta < 1.3'$. The survey depth enabled findings of galaxies with luminosities greater than $0.01 - 1.0\ L_*$ and impact parameters less than $100 - 350\ h^{-1}$ kpc at the redshifts $0.1 \lesssim z_{\rm gal} \lesssim 0.6$. The galaxy sample is therefore ideally suited for our present study.

Galaxies in the field of PKS 1622+2352 were first published in Steidel et al. (1997) as part of a program to determine the redshifts of galaxies found in deep Hubble Space Telescope (HST) images that are brighter than $R \approx 24.5$. Images of individual galaxies were also analyzed by Chen et al. (1998). Galaxies in the field of HE 0226−4110 were observed in an on-going program to uncover galaxies brighter than R = 23 mag at $z_{\rm gal} < 0.5$ for understanding the cross-correlation between galaxies and O VI $\lambda\lambda$1031, 1037 absorbers (Chen et al. 2008 in preparation). The two galaxy samples satisfy the selection criterion of an unbiased galaxy survey in QSO fields that does not rely on known knowledge of the presence of an Mg II absorber. We therefore include the galaxy data in our sample. Images of the galaxies are presented in Figure 2. The data were obtained using the Wide Field and Planetary Camera 2 (WFPC2) and the F702W filter (see also Chen et al. 2001a) on board HST, with the exception of the images of galaxies in the field around HE 0226−4110 that were obtained using IMACS and the *R*-band filter on the Magellan Baade telescope.

The sample of galaxies identified at $\rho \lesssim 100\ h^{-1}$ kpc from the lines of sight toward seven background QSOs is presented in Table 2, where we list for each galaxy in columns (1)—(7) the field, Right Ascension and Declination offsets from the QSO $\Delta\alpha$ and $\Delta\delta$, redshift $z_{\rm gal}$, impact parameter ρ, apparent *R*-band magnitude, and absolute *B*-band magnitude $M_B - 5\log h$.[3] Measurement uncertainties in *R* and $M_B - 5\log h$ were typically 0.2 dex. Our initial galaxy sample consists of 23 galaxies at redshifts from $z_{\rm gal}$ = 0.2067 to $z_{\rm gal}$ = 0.892 with a median of $z_{\rm gal}$ = 0.3818[4]. We have excluded galaxies that are within $|\Delta v| < 3000$ km s^{-1} from the background QSOs, where most of the gas is expected to be highly ionized due to the QSO proximity effect (e.g. Bajtlik et al. 1988). The rest-frame *B*-band magnitudes of the galaxies range from $M_B - 5\log h = -15.9$ to -20.3 with a median of $M_B - 5\log h = -19.0$, corresponding to $0.5L_{B_*}$ for $M_{B_*} - 5\log h = -19.8$ that characterizes the blue galaxy population at $z_{\rm gal} \sim 0.4$ (e.g. Faber et al. 2007).

3.3. *The Galaxy–Mg II Absorber Pair Sample*

To establish a galaxy–Mg II absorber pair sample for the subsequent analysis, we examine the echelle spectra of the background QSOs and search for the corresponding Mg II absorption doublet at the locations of the galaxies presented in § 3.2. Specifically, we accept absorption lines according to a 3σ detection threshold criterion, which is appropriate because the measurements are performed at a small number of known galaxy redshifts. Next, we form galaxy and absorber pairs by requiring a velocity difference[5] $\Delta v \leq 250$ km s^{-1}. Finally, we measure 3-σ upper limits to the 2796-Å absorption equivalent widths of galaxies that are not paired with corresponding absorbers. The procedure identifies 13 galaxy and absorber pairs and 10 galaxies that do not produce Mg II absorption lines to within sensitive upper limits. Impact parameter separations of the galaxy and absorber pairs range from ρ = 16.3 to 100.1 h^{-1} physical kpc with a median of ρ = 54.8 h^{-1} kpc. The corresponding Mg II absorption strength of each of the 23 galaxies in our sample is listed in columns (8)—(9) of Table 2.

[2] see http://web.mit.edu/~burles/www/MIKE/mike_cookbook.html.

[3] All magnitudes presented in this paper are in the *AB* system.

[4] We note that 12 of the 23 galaxies in our sample are from the field around 3C336. These 12 galaxies have spectroscopic redshifts evenly distributed from z = 0.261 to z = 0.892 with a median of $\langle z \rangle$ = 0.6, covering a comoving distance of $\approx 1.4\ h^{-1}$ Gpc. Therefore these galaxies are not part of a coherent structure. There is no known galaxy clusters along the sightline toward 3C336 and there is no physical mechanism that suggests that slight overdensities on scales of 0.1-1 Gpc would affect gas properties within individual halos.

[5] We note that the galaxy at $z_{\rm gal}$ = 0.4592 in the field around 1354+1933 is ≈ 550 km s^{-1} from the identified Mg II absorber. However, including the redshift measurement uncertainty of 300 km s^{-1} reported in Ellingson et al. (1991), we consider this pair a match.

TABLE 1
SUMMARY OF THE ECHELLE SPECTROSCOPIC OBSERVATIONS OF DISTANT QSOS

Field	RA(J2000)	Dec(J2000)	z_{QSO}	V	Instrument	Exptime	Spectral Coverage
PKS 0122–0021	01:25:28.8	–00:05:56	1.0765	16.4	MIKE	1200	3350–9400
HE 0226–4110	02:28:15.2	–40:57:16	0.4950	15.2	MIKE	600	3350–9400
PKS 0349–1438	03:51:28.5	–14:29:09	0.6163	16.2	MIKE	1800	3350–9400
PKS 0454–2203	04:56:08.9	–21:59:09	0.5335	16.1	MIKE	2700	3350–9400
PKS 1354+1933	13:57:04.4	+19:19:07	0.7200	16.0	UVES	600	3300–6800
PKS 1424–1150	14:27:38.1	–12:03:50	0.8060	16.5	UVES	720	3300–6600
3C336	16:24:39.1	+23:45:12	0.9274	17.5	UVES	14,700	3300–6600

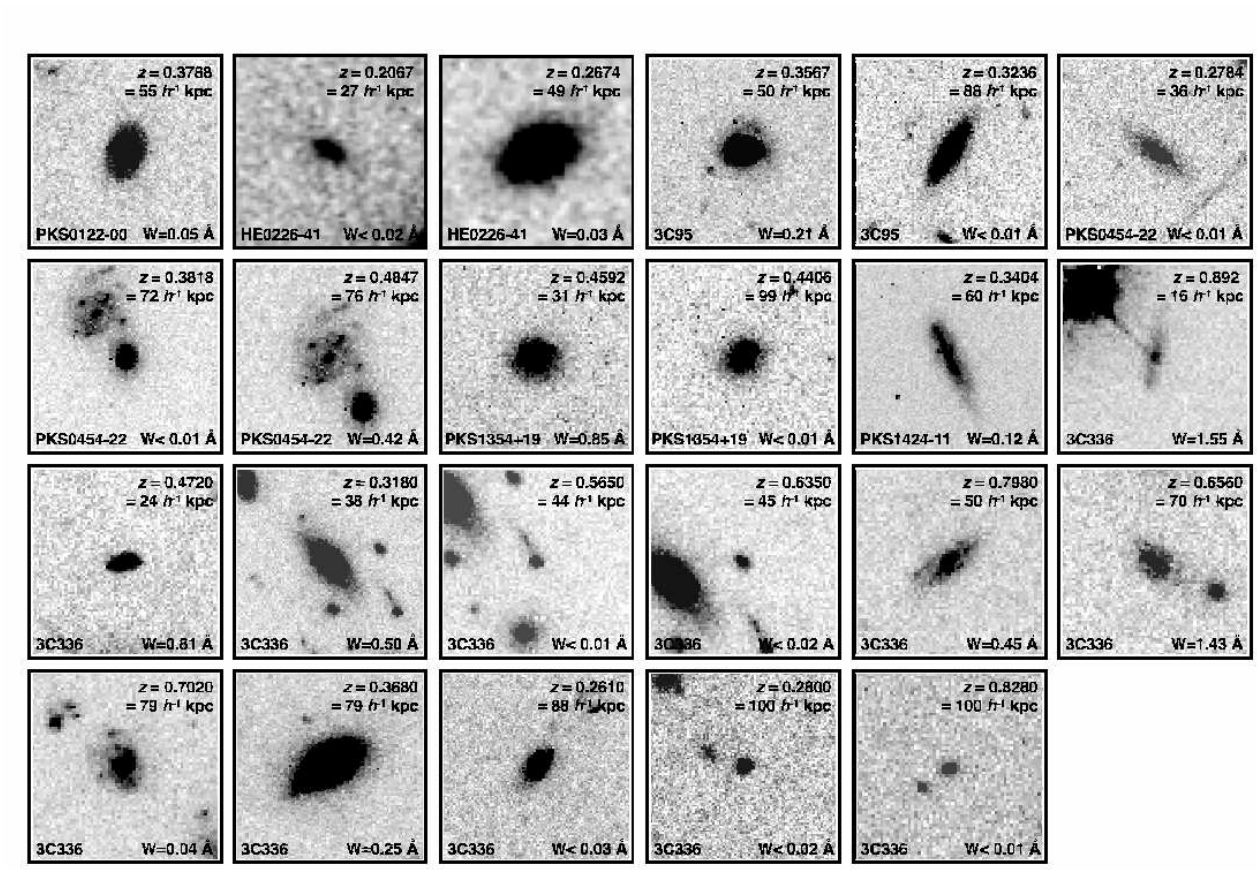

FIG. 2.— Images of the 23 galaxies in our sample that are identified at $\rho \lesssim 100\ h^{-1}$ kpc from the lines of sight toward a background QSO. With the exception of the two galaxies in the field of HE 0226–4110, the galaxy images were obtained using WFPC2 and the F702W filter (see also Chen et al. 2001a). Images of the galaxies in the field of HE 0226–4110 were obtained using IMACS and the *R* filter on the Magellan Baade telescope. The spatial extent of each image is roughly $25\ h^{-1}$ physical kpc on a side at the redshift of the galaxy indicated in the upper right-corner. The orientation of each image is arbitrary. The absorption strength of the corresponding Mg II absorbers found in the spectra of the background QSO described in § 3.1 is indicated in the lower-right corner. For non-detections, we provide a 3-σ upper limit to the rest-frame absorption equivalent width.

4. THE EXTENT AND COVERING FACTOR OF MG^+ IONS IN GALACTIC HALOS

In this section, we examine the correlation between galaxies and Mg II absorbers identified along common lines of sight, using the sample of 13 galaxy–Mg II absorber pairs and 10 galaxies at $\rho \lesssim 100\ h^{-1}$ kpc that do not give rise to Mg II absorption to a sensitive upper limit. The choice of $r_0 = 100\ h^{-1}$ kpc in selecting galaxies at $\rho \lesssim r_0$ for our analysis is adopted, in order to minimize the contamination of galaxies that are correlated with the true Mg II absorbing galaxies through clustering and to maximize the fraction of physical galaxy and absorber pairs in our sample. In addition to the simulation results presented in § 2, this criterion is further supported by the stronger clustering signal at small ($\rho < 100\ h^{-1}$ kpc) impact parameters of LRGs (Bouché et al. 2004). This strong signal is a natural consequence of cross-correlating objects inside

TABLE 2
GALAXIES AND ABSORPTION SYSTEMS

	Galaxies						Absorption Systems	
Field	$\Delta\alpha$ (arcsec)	$\Delta\delta$ (arcsec)	z_{gal}	ρ (h^{-1} kpc)	R^a	M_B $-5\log h$	z_{abs}	$W(2796)$ (Å)
(1)	(2)	(3)	(4)	(5)	(6)	(7)	(8)	(9)
0122–0021	–8.7	–12.3	0.3788	54.8	20.6	–19.2	0.3791	0.05 ± 0.01
0226–4110	–7.9	–7.9	0.2067	26.5	22.2	–16.4	...	< 0.02
	11.6	–12.5	0.2674	49.0	20.4	–18.4	0.2678	0.03 ± 0.01
0349–1438	–9.4	10.8	0.3567	50.1	20.6	–19.1	0.3572	0.21 ± 0.01
	11.7	–24.1	0.3236	88.0	20.0	–19.1	...	< 0.01
0454–2203	10.6	5.7	0.2784	35.6	21.1	–18.0	...	< 0.01
	–1.1	–18.0	0.4847	75.8	20.1	–20.3	0.4834	0.42 ± 0.01
	0.3	–19.7	0.3818	72.0	20.8	–19.1	...	< 0.01
1354+1933	1.2	7.5	0.4592	31.0	21.0	–19.3	0.4563	0.85 ± 0.01
	–21.6	–12.2	0.4406	98.8	20.9	–19.1	...	< 0.01
1424–1150	–0.2	17.6	0.3404	59.8	20.5	–19.1	0.3415	0.12 ± 0.04
3C336	3.0	–0.0	0.8920	16.3	23.3	–19.0	0.8909	1.55 ± 0.01
	–4.2	–3.8	0.4720	23.6	22.5	–17.9	0.4716	0.81 ± 0.01
	–5.5	7.5	0.6350	44.7	24.1	–17.1	...	< 0.02
	–8.9	3.2	0.7980	49.9	22.4	–19.5	0.7969	0.45 ± 0.01
	–3.3	9.1	0.5650	44.1	23.8	–17.1	...	< 0.01
	–6.7	9.7	0.3180	38.3	20.2	–18.9	0.3172	0.50 ± 0.01
	1.6	14.2	0.6560	69.6	22.7	–18.6	0.6556	1.43 ± 0.01
	–12.3	9.9	0.7020	79.1	21.9	–19.6	0.7023	0.04 ± 0.01
	7.9	–17.0	0.8280	99.7	24.2	–18.3	...	< 0.01
	–21.3	–6.2	0.3680	79.2	19.9	–19.9	0.3677	0.25 ± 0.01
	–24.1	5.3	0.3680	81.0	23.4	–16.4	...	...
	25.5	17.6	0.2610	87.5	21.6	–17.3	...	< 0.03
	12.7	–31.2	0.2800	100.1	22.9	–15.9	...	< 0.02

[a]The R magnitudes presented here were measured in HST/WFPC2 F702W filter for all galaxies but the two in the field around HE0226–4110. No filtered HST images are available for the field of HE0226–4110. The magnitudes were determined based on a ground-based image obtained with the Magellan Baade telescope using IMACS and the Johnson R filter.

the same dark matter halos of the LRGs.

To examine the existence of a fiducial relationship between the strength of Mg II absorption and galaxy impact parameter, we present in Figure 3 the distribution of $W(2796)$ with respect to ρ. Circles represent elliptical or S0 galaxies, triangles represent early-type spiral galaxies, and squares represent late-type spiral galaxies. Galaxy morphological types are adopted from the classifications of Chen et al. (1998, 2001a) that were based on a 2D surface profile analysis of the high resolution HST/WFPC2 images. We have also classified the galaxy at $(-7.9'', -7.9'')$ and the galaxy at $(11.6'', -12.5'')$ from the QSO HE 0226–4110 as a late-type and an early-type spiral galaxy based on their respective spectral features. Points with arrows in Figure 3 indicate 3σ upper limits.

Figure 3 shows that there is a moderate anti-correlation between $W(2796)$ and ρ, i.e. weaker Mg II absorption strength is observed for galaxies at larger impact parameter. We note that the obvious outlier of a Mg II absorber with $W(2796) = 1.43 \pm 0.01$ Å at $z = 0.656$, currently assigned to a galaxy at $\rho = 69.6\ h^{-1}$ kpc, is a known damped Lyα absorber of $\log N(\mathrm{H\,I}) = 20.36 \pm 0.08$ (Steidel et al. 1997; Rao et al. 2006). Although the galaxy satisfies our sample selection criterion, it is unlikely that the galaxy at $\rho = 69.6\ h^{-1}$ kpc is physically related to the absorber due to the large neutral gas content for two reasons. First, all radio detected sources in non-cluster environment from deep 21cm surveys have coincident optical counterparts (e.g. Doyle et al. 2005). Second, deep 21cm observations of the M 31 halo reveal no H I clouds of $N(\mathrm{H\,I}) > 10^{20}$ cm^{-2} (e.g. Thilker et al. 2004). This is also roughly consistent with the expected contamination rate at this projected separation presented in Figure 1.

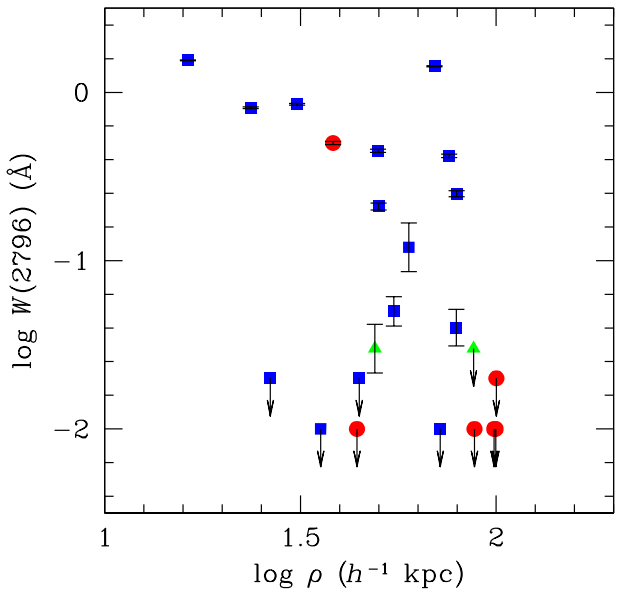

FIG. 3.— Comparison of the corresponding rest-frame absorption equivalent width $W(2796)$ versus galaxy impact parameter ρ for a sample of 23 galaxies. Circles represent elliptical or S0 galaxies, triangles represent early-type spiral galaxies, and squares represent late-type spiral galaxies. Points with arrows indicate 3σ upper limits.

To assess the significance of this anti-correlation, we perform a generalized Kendall test that accounts for the presence of non-detections and find that the null hypothesis, in which $W(2796)$ is randomly distributed with respect to ρ, can be ruled out at a $> 97\%$ confidence level. However, the scatter of the $W(2796)$ vs. ρ anti-correlation is clearly large. Specifically, 10 of the 23 galaxies at $\rho \lesssim 100\ h^{-1}$ kpc do not produce a corresponding Mg II absorber to a sensitive upper limit, implying a mean covering factor of the Mg^+ ions $\langle\kappa\rangle \approx 57$ % at $\rho < 100\ h^{-1}$ kpc. At $\rho < 45\ h^{-1}$ kpc, we find $\langle\kappa\rangle \approx 50$ %, similar to the preliminary result reported in Tripp & Bowen (2005).

We note, however, that the rest-frame B-band magnitudes of the galaxies range from $M_B - 5\log h = -15.9$ to -20.3 with a median of $M_B - 5\log h = -19.0$, corresponding to a range in intrinsic B-band luminosity from $0.03 L_{B_*}$ to $1.6 L_{B_*}$ with a median of $0.5 L_{B_*}$ for $M_{B_*} - 5\log h = -19.8$ at $z_{\rm gal} \sim 0.4$ (e.g. Faber et al. 2007). Because more massive galaxies are expected to reside in more massive halos and therefore possess larger gaseous halos, we examine whether accounting for galaxy intrinsic luminosity can improve upon the anti-correlation displayed in Figure 3.

Following TC08, we adopt an isothermal profile of finite extent $R_{\rm gas}$ for representing the density of the Mg^+ ions around individual galaxies. The expected Mg II absorption equivalent width, $\bar{W}$ as a function of galaxy impact parameter can be calculated following

$$\bar{W}(2796) = \frac{\bar{W}_0}{\sqrt{\rho^2 + a_h^2}} \tan^{-1} \sqrt{\frac{R_{\rm gas}^2 - \rho^2}{\rho^2 + a_h^2}} \qquad (1)$$

at $\rho \leq R_{\rm gas}$ and $\bar{W}(2796) = 0$ otherwise. The core radius a_h is defined to be $a_h = 0.2 R_{\rm gas}$ and does not affect the expected $\bar{W}(2796)$ at large ρ. The extent of Mg II absorbing gas scales with the luminosity of the absorbing galaxy according to

$$\frac{R_{\rm gas}}{R_{\rm gas*}} = \left(\frac{L_B}{L_{B_*}}\right)^{\beta}. \qquad (2)$$

Following the definition of Equation (2), $R_{\rm gas*}$ characterizes the gaseous extent of L_* galaxies. The gaseous extent of fainter/more luminous galaxies differs from $R_{\rm gas*}$ according the scaling relation.

To determine the values of $\bar{W}_0$, $R_{\rm gas*}$, and β that best describe the data, we perform a maximum-likelihood analysis that includes the upper limits in our galaxy and Mg II absorber pair sample. The likelihood function of this analysis is defined as

$$\mathcal{L} = \left(\prod_{i=1}^{n} \exp\left\{-\frac{1}{2}\left[\frac{y_i - \bar{y}(\rho_i, L_{B_i})}{\sigma_i}\right]^2\right\}\right) \times \left(\prod_{i=1}^{m} \int_{y_i}^{-\infty} dy' \exp\left\{-\frac{1}{2}\left[\frac{y' - \bar{y}(\rho_i, L_{B_i})}{\sigma_i}\right]^2\right\}\right), \qquad (3)$$

where $y_i = \log W_i$, $\bar{y} = \log \bar{W}$, and σ_i is the measurement uncertainty of y_i. The first product of Equation (3) extends over the n measurements and the second product extends over the m upper limits. (This definition of the likelihood function is appropriate if the residuals about the mean relationship are normally distributed.) Because σ_i may include significant intrinsic scatter (which presumably arises due to intrinsic variations between individual galaxies) as well as measurement error, σ_i is taken to be the quadratic sum of the cosmic scatter σ_c and the measurement error σ_{m_i}

$$\sigma_i^2 = \sigma_c^2 + \sigma_{m_i}^2, \qquad (4)$$

where the intrinsic scatter is defined by

$$\sigma_c^2 = \mathrm{med}\left(\left\{y_i - \bar{y}(\rho_i, L_{B_i}) - \frac{1}{n}\sum_{j=1}^{n}\left[y_j - \bar{y}(\rho_j, L_{B_j})\right]\right\}^2 - \sigma_{m_i}^2\right). \qquad (5)$$

Because σ_c depends on the maximum-likelihood solution $\bar{y} = \log \bar{W}(\rho_i, L_{B_i})$, the maximum-likelihood solution is obtained iteratively with respect to equations (1) and (2). The maximum-likelihood analysis yields

$$\beta = 0.35 \pm 0.05, \qquad (6)$$

and

$$R_{\rm gas*} = 91^{+3}_{-8}\ h^{-1}\ \mathrm{kpc}, \qquad (7)$$

and $\bar{y}_0 = \log \bar{W}_0 = -0.25 \pm 0.05$ for the best-fit $R_{\rm gas*}$. The errors represent the 1-σ uncertainties of the best-fit parameters. In addition, we estimate a cosmic scatter of $\sigma_c = 0.25$ dex. The best-fit isothermal model is presented in Figure 4 (solid curve).

The results of our maximum likelihood analysis indicate that the extent of Mg II gaseous halo scales with galaxy B-band luminosity according to $(L_B/L_{B_*})^{\beta}$ and $\beta = 0.35 \pm 0.05$, and that typical L_* galaxies possess an extended Mg II halo of radius $R_{\rm gas} \approx 91\ h^{-1}$ kpc. It is worth noting that the best-fit $91^{+3}_{-8}\ h^{-1}$ kpc characterizes the gaseous extent of L_* galaxies, beyond which no Mg^+ ions are found to the limit of

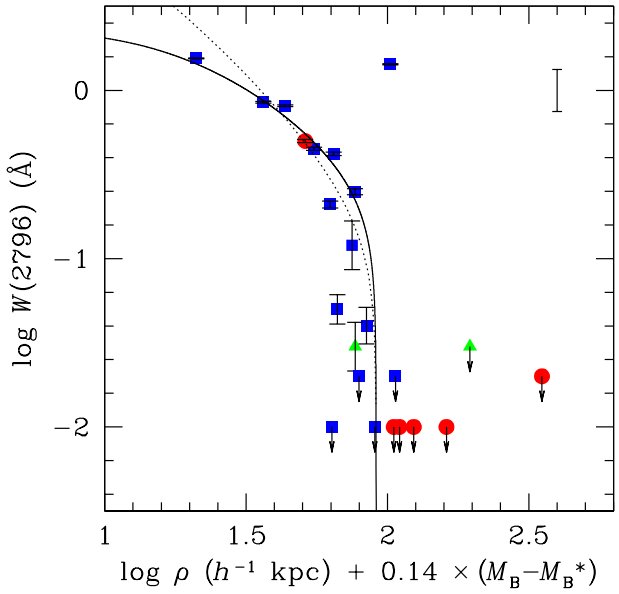

FIG. 4.— Comparison of the rest-frame absorption equivalent width $W(2796)$ versus galaxy impact parameter ρ scaled by galaxy B-band luminosity. Symbols are the same as those in Figure 3. The solid curve represents the best-fit model based on an isothermal density profile of the Mg^+ ions, while the dotted curve shows the expectation from an NFW density profile. The errorbar in the upper-right corner represents the intrinsic scatter of the best-fit model, in comparison to the observations, as defined in Equation (5).

$W_r(2796) = 0.01$ Å. Adopting the best-fit scaling relation, the gaseous extent of $0.1L_*$ galaxies is expected to be $\approx 41\ h^{-1}$ kpc. Figure 4 shows the relation of $W_r(2796)$ vs. luminosity scaled ρ, in which seven galaxies at $> 100\ h^{-1}$ kpc do not have a corresponding Mg II absorption feature to the limit of $W(2796) = 0.01$ Ang. These non-detections provide the strongest constraints on $R_{\rm gas*}$.

To examine possible bias in $R_{\rm gas*}$ as a result of the initial sample definition that consider only galaxies at $\rho \lesssim r_0 = 100\ h^{-1}$ kpc, we repeat the likelihood analysis adopting $r_0 = 80\ h^{-1}$ kpc and find that the best-fit results remain the same. Choosing a smaller r_0 reduces the sample substantially and the parameters become poorly constrained. Furthermore, we note that the results are also insensitive to the choice of model gaseous profile. We obtain similar results, adopting a Navarro-Frenk-White (NFW) profile commonly used for describing the profiles of dark matter halos (Navarro et al. 1997). The best-fit NFW profile is also presented in Figure 4 (dotted curve). Comparisons of observations and different model profiles show that an isothermal model profile of the underlying gaseous halo provides a good fit to the observed $W(2796)$ vs. ρ relation.

In summary, Figure 4 demonstrates that accounting for the scaling relation of gaseous extent with galaxy luminosity, the scatter in the $W(2796)$ versus ρ relation is substantially reduced. Furthermore, the $W(2796)$ versus ρ relation scaled by galaxy intrinsic luminosity allows us to estimate a mean covering factor of Mg^+ ions average across galaxies of a wide range of luminosity. We find $\langle\kappa\rangle = 80-86$ % within $R_{\rm gas}$, including the uncertainty in $R_{\rm gas*}$ from Equation (7).

5. DISCUSSION

Using the sample of 13 galaxy–Mg II absorber pairs and 10 galaxies at $\rho \lesssim 100\ h^{-1}$ kpc that do not give rise to Mg II absorption to a sensitive upper limit, we find that galaxies at larger impact parameters produce on average weaker Mg II absorbers. This anti-correlation is substantially improved, when accounting for the intrinsic luminosity of individual galaxies. In addition, there exists a distinct boundary at $\rho = R_{\rm gas}$, beyond which no Mg II absorbers with $W(2796) \geq 0.01$ Å are found. A maximum likelihood analysis shows that the observations are best described by an isothermal density profile of the gas and a scaling relation $R_{\rm gas} = 91^{+3}_{-8} \times (L_B/L_{B_*})^{(0.35\pm0.05)}\ h^{-1}$ kpc with a mean covering factor of $\langle\kappa\rangle = 80-86$ % at $\rho \leq R_{\rm gas}$. The best-fit profile applies to galaxies of $0.03L_{B_*}$ to $1.6L_{B_*}$ and therefore predominantly cold-mode halos. For higher mass halos, we expect from TC08 that the corresponding absorption strength for a given ρ is reduced, namely a smaller $\bar{W}_0$ in Equation (1). In this section, we discuss the implications drawn from the results of our analysis.

5.1. *Comparisons with Previous Studies*

Adopting the best-fit scaling relation and the gaseous profile described in Equation (1), we derive a corresponding halo size of $\rho \approx 69\ h^{-1}$ physical kpc for galaxies of $M_B - 5\log h = -19.8$ at $W(2796) = 0.3$ Å. This halo size is consistent with the finding of Lanzetta & Bowen (1990) and the expectation inferred from known Mg II frequency function (Nestor et al. 2005; see the descriptions in § 5.2), but is larger than what was reported in Steidel (1995). Steidel (1995) reported a characteristic size of Mg II halo of $R_* \approx 35\ h^{-1}$ kpc for L_* (corresponding to $M_{B_*} - 5\log h = -19.7$ for the cosmology adopted in this paper) galaxies, but it is not clear at what $W(2796)$ limit the halo size was estimated. At $\rho = 35\ h^{-1}$ kpc, we expect $\bar{W}(2794) = 0.9$ Å from the best-fit model.

The high gas covering factor derived from our analysis is consistent with what is inferred from the sample of Kacprzak et al. (2008). Applying the best-fit luminosity scaling relation of gaseous extent, we find that four of the 28 galaxies within the expected gaseous extent for $W_r(2796) > 0.3$ Å absorbers in the Kacprzak et al. sample have a corresponding Mg II weaker than the 0.3 Å threshold. The inferred covering fraction is ≈ 86%. At the same time, this high covering fraction disagrees with the value reported in Tripp & Bowen (2005), the only other on-going survey program designed to constrain gas covering fraction by searching for corresponding Mg II absorbers at the locations of known *field* galaxies[6]. The authors obtained follow-up spectra of background QSOs that are located within $\rho = 10-39\ h^{-1}$ physical kpc of 20 known galaxies at $z_{\rm gal} = 0.31-0.55$. They found that 10 of the 20 galaxies do not produce Mg II absorbers to within a 2-σ upper limit of $W(2796) = 0.1$ Å, and concluded that the incidence of Mg^+ ions is ≈ 50 % at $\rho \lesssim 40\ h^{-1}$ kpc in individual galactic halos.

Because more luminous galaxies have larger extended Mg II halos according to the scaling relation presented in Equations (2), (6), and (7), this discrepancy can be understood if many of the galaxies in Tripp & Bowen are located at impact parameters that are larger than their expected $R_{\rm gas}$. Recall that we obtained a similar estimate of $\langle\kappa\rangle \approx 57$ % at $\rho < 100\ h^{-1}$ kpc (or $\langle\kappa\rangle \approx 50$ % at $\rho < 45\ h^{-1}$ kpc), *prior to* accounting for the scaling relation between $R_{\rm gas}$ and L_B in individual galaxies (§ 4).

In addition, the sample in Tripp & Bowen includes galaxies of luminosity ranging from $0.3L_*$ to $5L_*$. Those galaxies that are more luminous than L_* are also expected to reside in more massive halos. At $z = 0$, $5L_*$ galaxies are expected to reside in $> 10^{13} h^{-1}\,{\rm M}_\odot$ halos (Tinker et al. 2007). If the host dark matter halos are substantially more massive than $10^{12.0} h^{-1}\,{\rm M}_\odot$, then we expect from the halo occupation analysis in TC08 that they do not contribute significantly to strong Mg II absorbers. In summary, further inspections of the properties of these galaxies and estimates of the gas covering fraction κ as a function of radius and $W(2796)$ are crucial for resolving this discrepancy.

5.2. *The Origin of Mg II Absorbers*

The scaling relation and the constraint of $\langle\kappa\rangle$ together also allow us to test whether the Mg II absorbers trace a significant and representative portion of the galaxy population or merely a special class such as those galaxies undergoing a starburst episode. If extended Mg II halos are a generic feature of field[7] galaxies at all epochs, then we can derive the expected number density of Mg II absorbers by combining known space density of galaxies (versus luminosity) and the product of the cross section and covering factor of the Mg^+ ions. An agreement with observational results from surveys of Mg II absorbers

[6] We note two earlier surveys by Bechtold & Ellingson (1992) and Bowen et al. (1995) that include a dominant fraction of galaxies in dense cluster environment. Both studies reported a substantially lower covering fraction, $\langle\kappa\rangle \lesssim 20$ % for $W(2796) > 0.1$ absorbers. The low covering fraction of strong absorbers is understood, because galaxies clusters reside in massive dark matter halos of $M_h > 10^{14} h^{-1}\,{\rm M}_\odot$ and the fraction of "cold" gas in these massive halos is expected to be reduced (see TC08).

[7] We define field galaxies as those that are not associated with a known cluster.

would challenge the scenario that attributes a large fraction of these absorbers to starburst systems[8].

The predicted number density of Mg II absorption systems arising in the extended gaseous halos of galaxies may be evaluated according to

$$\frac{d\mathcal{N}(W \geq W_{lim})}{dz} = \frac{c}{H_0} \frac{(1+z)^2}{\sqrt{\Omega_{\rm M}(1+z)^3+\Omega_\Lambda}} \times \int_0^\infty d\left(\frac{L_B}{L_{B_*}}\right) \Phi(L_B,z)\,\sigma(L_B,W_{lim})\,\kappa, \quad (8)$$

where c is the speed of light, $\Phi(L_B,z)$ is the galaxy luminosity function, σ is the gas cross section for producing Mg II absorbers of $W(2796) \geq W_{lim}$ that scales with galaxy B-band luminosity, and κ is the halo covering factor. Substituting the scaling relationship according to Equations (2), (6), and (7), we find

$$\frac{d\mathcal{N}(W \geq W_{lim})}{dz} = \frac{c}{H_0} \frac{\pi\,\langle\kappa\rangle\,[R'_{\rm gas*}(W_{lim})]^2\,(1+z)^2}{\sqrt{\Omega_{\rm M}(1+z)^3+\Omega_\Lambda}} \times \int_0^\infty d\left(\frac{L_B}{L_{B_*}}\right)\left(\frac{L_B}{L_{B_*}}\right)^{2\beta} \Phi(L_B,z), \quad (9)$$

where $R'_{\rm gas*}(W_{lim})$ is the extent of Mg II halos that corresponds to $W(2796) = W_{lim}$.

To evaluate Equation (9), we adopt the luminosity function of the blue galaxy population at $z_{\rm gal} = 0.3-0.5$ from Faber et al. (2007), which is characterized by $M_{B_*} - 5\log = -19.8$, $\phi_* = 9.6\times10^{-3}\ h^3$ Mpc^{-3}, and a faint-end slope $\alpha = -1.3$. Including galaxies of $L_B \geq 0.01\,L_{B_*}$ and our best-fit $R_{\rm gas*}$ and $\langle\kappa\rangle$, Equation (9) yields $d\mathcal{N}/dz = 0.028-0.03$ for $W(2796) \geq 2$ Å absorbers, $d\mathcal{N}/dz = 0.21-0.23$ for $W(2796) \geq 1$ Å absorbers, and $d\mathcal{N}/dz = 0.88-1.07$ for $W(2796) \geq 0.3$ Å absorbers at $z = 0.5$. The predictions based on galaxies more luminous than $0.01\,L_*$ agree well with the observed $d\mathcal{N}/dz$ from Nestor et al. (2005), lending strong support for the hypothesis that the Mg II absorbers trace a significant and representative portion, rather than a sub-class, of the galaxy population.

The model profile of Equation (1) has been proved to be a good representation of the galaxy and absorber pairs at $\rho = 16.3-100\,h^{-1}$ kpc, when the scaling relation of Equations (2), (6), and (7) is accounted for. An important test is to examine whether the model remains a good fit at smaller ρ and strong absorbers. Identifying galaxy–absorber pairs at small impact parameters is difficult, because the glare of the background QSO often prohibits identification of faint galaxies at angular distances $\theta < 2''$ that corresponds to $\sim 10\,h^{-1}$ physical kpc at $z \lesssim 0.5$.

Recent studies of intervening absorption-line systems along the lines of sight toward the optical afterglows of distant γ-ray bursts (GRB) have uncovered a number of strong Mg II absorbers (e.g. Prochter et al. 2006b). Unlike QSOs, GRB afterglows disappear after a while, permitting exhaustive searches of faint galaxies at $\theta < 2''$ that give rise to strong Mg II absorbers along the lines of sight. A redshift survey of galaxies along the sightline toward GRB 060418 ($z_{\rm GRB} = 1.491$) has uncovered the absorbing galaxies for three strong Mg II absorbers at $z = 0.603-1.107$ (Pollack et al. 2008, in preparation), similar to the redshift range covered by our sample. The rest-frame B-band magnitudes of the galaxies range from $M_B - 5\log h = -16.8$ to $M_B - 5\log h = -18.3$; Impact parameters of the galaxies range from $\rho = 7.5\ h^{-1}$ kpc to $\rho = 16.5\ h^{-1}$ kpc. Adopting the best-fit scaling relation, we include the three galaxy–Mg II absorber pairs in the $W(2796)$ versus ρ plot for comparison (star points in Figure 5). The good agreement between the best-fit model and the absorbers found along GRB sightlines provides further support for our model at small impact parameters.

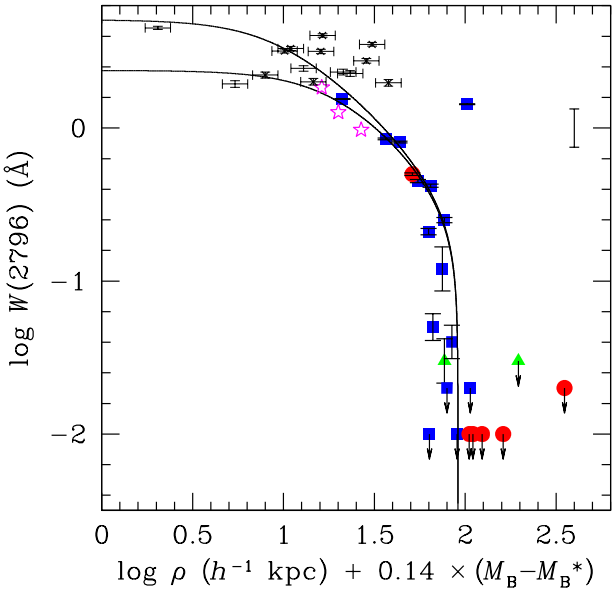

FIG. 5.— The $W(2796)$ versus ρ correlation scaled by galaxy B-band luminosity presented in Figure 4, but including pairs from Pollack et al. (2008; star points) and Bouché et al. (2007; points with horizontal errorbars) for comparisons. The solid curves represent the best-fit model based on an isothermal density profile, with $a_h = 0.1\,R_{\rm gas}$ (top curve) and $a_h = 0.2\,R_{\rm gas}$ (bottom curve). The pairs of Pollack et al. are for galaxies and Mg II absorbers identified at $z = 0.6-1$ along the sightline toward GRB 060418. The errorbars in these data points are smaller than the size of the symbols. The pairs of Bouché et al. are galaxies found at the positions of known Mg II absorbers based on the presence of Hα emission lines. Errorbars represent the uncertainties of the inferred M_B from the M_B versus L(Hα) correlation published in Tresse et al. (2002). Crosses represent the absorbers in the Bouché sample that are likely ($\gtrsim 40$ % probability) to be a damped Lyα absorber of N(H I) $\geq 2\times10^{20}$ cm^{-2} based on the presence of strong Fe II and Mg I transitions (Rao et al. 2006).

5.3. *Are Strong [$W(2796) > 1$ Å] Absorbers at $z \sim 1$ Produced Primarily in Starburst Outflows?*

As described in § 1, the large line width of $W(2796) > 1$ Å Mg II absorbers has recently been interpreted as due to outflow motions in starburst driven winds. This scenario was initially motivated by the observed inverse correlation between $W(2796)$ and the clustering amplitude of Mg II absorbers at $\langle z\rangle = 0.6$ (Bouché et al. 2006). In TC08, we have shown that this inverse correlation can be understood as due to an elevated clustering amplitude of $W(2796) \lesssim 1$ Å absorbers from contributions of survived cold clouds in massive hot halos, rather than a suppressed clustering strength of $W(2796) \gtrsim 2$

[8] However, we will not to able to rule out a scenario in which the blow-out winds are common in most galaxy histories. Given enough time, long-lived outflowing gas gets mixed in with existing halo gas and newly accreted material from the IGM. There is little distinction at this point between outflows and accreted clouds. It is also not clear whether the outflow material would maintain the same degree of complex gas kinematics as those that are closer to the parent starburst regions.

Å absorbers. In addition, we have shown in §§ 4, 5.1, and 5.2 that extended Mg II halos are a generic feature of field galaxies over a wide luminosity range. The predicted number density of the absorbers from adopting the scaling relation, Equations (2), (6), and (7), and the galaxy luminosity function agrees well with observations. Specifically, we expect $d\mathcal{N}/dz \approx 0.03$ for $W(2796) \geq 2$ Å absorbers, in comparison to the observed $d\mathcal{N}/dz = 0.03-0.04$ for $W(2796) \geq 2$ Å absorbers at $z \approx 0.5$ from Nestor et al. (2005). While there is no clear indicator one can apply to unambiguously distinguish between gas inflows and outflows in the distant universe, we discuss several caveats related to the starburst outflow scenario.

If the absorbers are produced in starburst driven outflows, then a large fraction of the absorbing galaxy population might be expected to exhibit disturbed morphology (Mobasher et al. 2004). The Mg II absorbing galaxies in our sample exhibit regular disk morphologies in the HST images shown in Figure 2. In particular, the strong absorber found with $W(2796) = 1.55$ Å at $z = 0.892$ toward 3C336 is associated with an edge-on disk galaxy at $\rho = 16.3\ h^{-1}$ kpc. The three Mg II absorbers of $W(2796) > 1$ Å found toward GRB 060418 also exhibit regular disk structures in high-resolution images obtained both in space using HST and on the ground using LGAO on the Keck telescopes (Pollack et al. 2008, in preparation). Kacprzak et al. (2007) also showed that there is little correlation between $W_r(2796)$ and galaxy asymmetry for Mg II absorbers of $W_r(2796) > 1.4$ Å. While some strong Mg II absorbers have been presented to show evidence of arising in expanding superbubble shells (Bond et al. 2001), available high-resolution images of other strong Mg II absorbers do not support outflow being principally responsible for the observed strong absorbers. This conclusion is also consistent with the spectral properties of Mg II-selected galaxies published by Guillemin & Bergeron (1997)

On the other hand, Bouché et al. (2007) presented new observations from a targeted search for corresponding Hα emission in the vicinity of known Mg II absorbers. These authors successfully identified Hα emission near 14 of 21 Mg II absorbers with $W(2796) > 1.9$ Å at $z \sim 1$. The integrated raw[9] Hα luminosities range from $L_{\mathrm{H}\alpha} = 6.8 \times 10^{40}\ h^{-2}$ erg s^{-1} to $L_{\mathrm{H}\alpha} = 8.4 \times 10^{41}\ h^{-2}$ erg s^{-1}. The impact parameters range from $\rho = 1.4\ h^{-1}$ kpc to $\rho = 35\ h^{-1}$ kpc. Adopting a mean extinction correction $A_V = 0.8$ mag, the authors inferred a mean star formation rate of $\langle \mathrm{SFR} \rangle = 5.9\ h^{-2}\ \mathrm{M}_\odot\ \mathrm{yr}^{-1}$ for these galaxies.

The Hα luminosity function at $z \sim 1$ has been studied by a number of groups (see Doherty et al. 2006 for a list of references). It is characterized by a Schechter function of $L_{\mathrm{H}\alpha_*} = 5 \times 10^{41}\ h^2$ erg s^{-1}, $\phi_* = 0.013\ h^3\mathrm{Mpc}^{-3}$, and $\alpha = -1.3$. The galaxies detected in Hα by Bouché et al. correspond to $0.14-1.68\,L_{\mathrm{H}\alpha_*}$ at $z \sim 1$, and therefore have only modest $L(\mathrm{H}\alpha)$. Integrating the Hα luminosity function, we obtain a mean space density of $0.034\ h^3$ Mpc^{-3} for galaxies of brighter than $0.1\,L_{\mathrm{H}\alpha_*}$. This is already 50% of all galaxies more luminous than $0.01\,L_{B_*}$ at $z \sim 1$, according to the best-fit luminosity function of the blue galaxy population from Faber et al. (2007). This exercise shows that Hα emission is commonly seen in $z \sim 1$ galaxies and the presence of modest $L(\mathrm{H}\alpha)$ does not argue for the presence of starburst outflows, unless the outflow material is long-lived.

For comparison, we include the 14 galaxy and absorber pairs from Bouché et al. (2007) in the $W(2796)$ versus ρ plot in Figure 5, applying the same scaling relation described in Equations (2), (6), and (7). We estimate M_B of these galaxies based on the published $M_B - L(\mathrm{H}\alpha)$ correlation in Tresse et al. (2002). We adopt the observed $L(\mathrm{H}\alpha)$ and the scaling relation $M_B = 73.5 - 2.27 \times \log L_(\mathrm{H}\alpha)$ that best describes the data in Tresse et al. (2002). At small impact parameters, the model predictions depend sensitively on the choice of a_h in Equation (1). In addition to the fiducial model, we also include in the figure a model with $a_h = 0.1\,R_{\mathrm{gas}}$.

Nine of the 14 Mg II absorbers are considered likely (> 40 %) damped Lyα absorbers (DLAs) of $N(\mathrm{H\,I}) \geq 2 \times 10^{20}$ cm^{-2} based on the presence of strong Fe II and Mg I transitions (Rao et al. 2006). DLAs are the high-redshift analog of neutral gas regions that resembles the disks of nearby luminous galaxies (e.g. Wolfe et al. 2005). We therefore expect that the impact parameter distribution of galaxy-DLA pairs represents the typical extent of H I disks at high redshifts. We highlight the potential DLAs in the Bouché et al. sample as crosses in Figure 5. After applying the best-fit scaling relation for Mg II absorbers, we find that the impact parameters of these galaxy and potential DLA pairs range from $8\ h^{-1}$ kpc to as high as $38\ h^{-1}$ kpc. The three largest separation pairs have $\rho' > 28\ h^{-1}$ kpc, where ρ' is the luminosity scaled projected distance. The scaling of impact parameter is justified, because smaller/fainter galaxies have on average smaller H I disks (e.g. Cayatte et al. 1994). The large impact parameters, together with the likely high $N(\mathrm{H\,I})$, suggest that the galaxies responsible for these absorbers (presumably at smaller angular distances from the QSOs) may still be missing. For the remaining sample, our model is in reasonably good agreement with their data.

In summary, we find a lack of empirical measurements that argue for starburst outflows to be a dominant mechanism for producing the observed strong Mg II absorbers at $z \sim 1$. On the other hand, both the observed number density of Mg II absorbers and the $W(2796)$ versus ρ correlation can be explained by extended Mg II halos around typical field galaxies. The fraction of Mg II absorbers originating in starburst outflows is therefore expected to be small at $z \sim 1$, unless starburst outflows are a common feature in field galaxies. We caution, however, that the same conclusion cannot be automatically applied to absorbers at $z \sim 2$ before a similar analysis is performed.

5.4. *Constraints on the Extended Gaseous Halos Around Galaxies*

The sharp decline of $W(2976)$ found at $\rho \approx 90\ h^{-1}$ kpc in Figure 4 clearly indicates that Mg^+ ions have a finite extent in the extended gaseous halos around galaxies. This is reminiscent of the sharp boundary between the C IV absorbing and non-absorbing regions around $\langle z \rangle = 0.4$ galaxies reported in Chen et al. (2001b).

Given the nature of a photo-ionized gas (Bergeron & Stasínska 1986; Hamann 1997), we examine whether the finite ex-

[9] No extinction correction is applied to $L(\mathrm{H}\alpha)$ in our analysis, because the dust content is expected to vary substantially in $z \sim 1$ galaxies (e.g. Tresse et al. 2002) and is unknown for galaxies in the Bouché et al. sample. Bouché et al. (2007) applied a constant correction to all observed Hα flux in their calculation, resulting in a simple scaling of the observed values. The scatter in their measurements induced by dust remains the same. For consistency, we consider in the following discussion only observed values without extinction correction both for the absorbing galaxies and for comparison results, such as the Hα luminosity function and the $M_B - L(\mathrm{H}\alpha)$ correlation, from the literature.

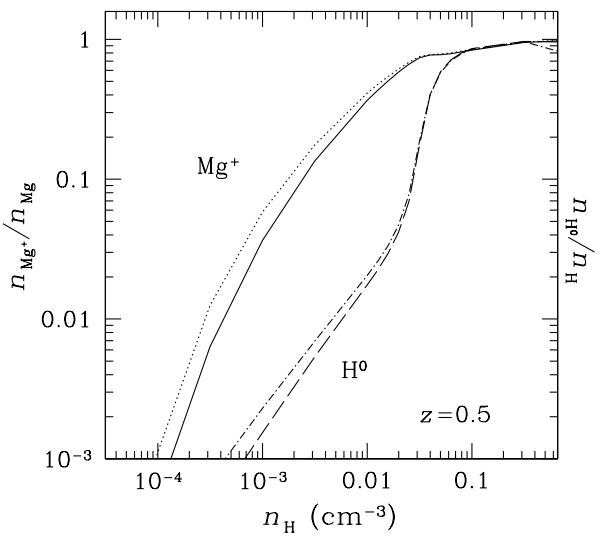

FIG. 6.— Ionization fractions of Mg^+ ions and H^0 atoms versus total gas density $n_{\rm H}$ for photo-ionized gas. The values are calculated using the Cloudy software (Ferland et al. 1998; version 06.02) for gaseous clouds of plane parallel geometry and 100 pc thickness. The input ionizing radiation intensity is set to be $J_\nu(912) = 7\times10^{-23}$ erg s^{-1} Hz^{-1} cm^{-2} Sr^{-1} suitable for the $z<1$ universe (Scott et al. 2002). We perform the calculations, assuming solar (dotted curve for Mg and dot-dashed curve for H) and $1/10$ solar metallicity (solid curve for Mg and dashed curve for H).

tent of Mg^+ ions can be understood as due to photo-ionization of the absorbing clouds at large radii. In a two-phase halo model (e.g. Mo & Miralda-Escudé 1996), cold clouds that are responsible for producing the absorption features are pressure confined in a hot medium. As the total gas density declines toward larger radii, the density of the cold clouds also decreases and the clouds become optically thin to the ultraviolet photons that can quickly ionize the Mg^+ ions (I.P. = 15.035 eV). With a known background radiation field, the location where the ionization transition occurs may be adopted to constrain the density of cold gas at large radii.

We carry out the photo-ionization analysis, using the Cloudy software (Ferland et al. 1998; version 06.02), and calculate the ionization fractions of Mg^+ ions for a grid of models with different total gas density and metallicity. We adopt the spectral shape of the UV background radiation field of Haardt & Madau in Cloudy for the incident ionizing flux, and scale the radiation intensity to the background UV radiation field inferred from QSO proximity effect (Scott et al. 2002). We adopt a plane parallel geometry for the clouds with a thickness of 100 pc, which is motivated by the observed coherent length of Mg II absorbers toward lensed QSOs (Rauch et al. 2002). The slab of gas is illuminated by the ionization radiation field on both sides.

Figure 6 shows the expected fractions of Mg^+ ions (solid and dotted curves) as a function of the total gas density $n_{\rm H}$. We include the calculated fraction of H^0 atoms (dashed and dash-dotted curves) for comparison. The solid and dashed curves are for gas of $1/10$ solar metallicity, while the dotted and dash-dotted curves are for gas of solar metallicity. Our photo-ionization calculations indicate that indeed the fraction of Mg^+ declines linearly at $n_{\rm H} \lesssim 0.025$ cm^{-3} for a mean radiation intensity of $J_\nu(912) = 7\times10^{-23}$ erg s^{-1} Hz^{-1} cm^{-2} Sr^{-1} (which is appropriate for the observed background radiation field at $z<1$ Scott et al. 2002). However, the transition is not as sharp as what is seen for hydrogen atoms. Including the estimated ionization fraction from the Cloudy models and adopting the density profile parameterized in Equation (1), we derive the expected correlation between $W_r(2796)$ and ρ and find that photo-ionization is insufficient for explaining the presence of the sharp decline in the observed Mg II absorption strength.

This extent of Mg II gaseous halos ($\approx 90\ h^{-1}$ kpc around typical L_* galaxies) is remarkably similar to the extent of C IV gaseous halo ($\approx 110\ h^{-1}$ kpc around typical L_* galaxies, after correcting for the Λ-cosmology) reported by Chen et al. (2001b). On the basis of 14 galaxy and C IV absorber pairs and 36 galaxies that do not produce corresponding C IV absorption lines to within sensitive upper limits, these authors find that the extent of C IV-absorbing gas around galaxies scales with galaxy B-band luminosity as $R_{\rm gas}({\rm C\,IV}) \propto 110\times L_B^{0.5\pm0.1}\ h^{-1}$ kpc (corrected for the Λ cosmology). In addition, there exists a sharp boundary between C IV absorbing and non-absorbing regions at $R_{\rm gas}$(C IV). But the scatter in the observed C IV absorption strengths at $\rho < R_{\rm gas}$(C IV) between different galaxies appears to be significantly larger than what is seen in Figure 4, and there is a lack of anti-correlation between the observed C VI absorbing strength and galaxy impact parameter.

Given the distinct ionization potentials of the C^{3+} and Mg^+ ions, *the location where the abrupt transition between absorbing and non-absorbing regions occurs can be understood as a critical radius below which cool clouds can form and stablize in an otherwise hot halo*. This two-phase model to interpret QSO absorption line systems was formulated in Mo & Miralda-Escudé (1996) and later re-visited by Maller & Bullock (2004).

Taking into account the appropriate photo-ionization condition of the cold clouds, Mo & Miralda-Escudé presented the expected Mg II and C IV absorption strength versus radius for halos of different mass. Their models showed a lack of radial dependence on the C IV absorption strength and a tight correlation between Mg II $W_r(2796)$ and ρ for halos of a wide range of mass. The differences in the radial dependence of different ions is understood as being due to the photo-ionization condition of cold clouds in the UV background radiation field. These model expectations agree with observational findings very well.

The agreement between observations and a simple two-phase model is encouraging, although it is not clear how the two-phase model applies to cold-mode halos (e.g. Dekel & Birnboim 2006). Measurements of the relative abundances between C^{3+} and Mg^+ as a function of radius will provide additional support for the origin of these metal-line absorbers, further constraining the metallicity and density of halo gas around galaxies.

5.5. *Implications for the Halo Occupation Analysis and Future Work*

Our initial halo occupation analysis (TC08) included two principal assumptions for the extent of Mg^+. First, we assumed that the extent of the cold gaseous halo is $R_{\rm gas,12} = 50\,h^{-1}$ physical kpc for $M_h = 10^{12}\,h^{-1}\,{\rm M}_\odot$ halos, which is roughly $1/3$ of the halo radius R_{200} at $z = 0.6$. Recall that the standard definition of a dark matter halo is an object with

a mean interior density of 200 times the background density. Second, the gaseous extent scaled with the halo mass as M_h^t and $t = 1/3$, following the expectation of the scaling relation between halo mass and the corresponding virial radius. The results presented in § 4 offer a direct test of these assumptions.

To compare the empirical constraints of Equations (6) & (7) with our initial model assumptions, we first derive the corresponding dark matter halo mass M_h and their halo radius R_{200} for galaxies of known absolute *B*-band magnitudes. The adopted M_{B_*} for the analysis in § 4 corresponds to a magnitude of $M_{b_J} - 5\log h = -19.7$ in the bandpass of the Two-Degree Field Galaxy Redshift Survey (2dFGRS, Colless et al. 2001). The 2dFGRS probes galaxies at $z \sim 0.1$. Excluding galaxies that exist as satellites in a cluster environment[10], the mean halo mass for M_{B_*} galaxies is $10^{12.5}\,h^{-1}\,h^{-1}\,M_\odot$ at $z \sim 0.1$ (Tinker et al. 2007; van den Bosch et al. 2007). At $z \sim 1$, galaxies of this magnitude on average reside in $10^{11.9}\,h^{-1}\,M_\odot$ halos (ZCZ07). Interpolating in $\log(1+z)$, we find that galaxies of $M_{B_*} - 5\log h = -19.8$ are expected to reside in halos of $M_h = 10^{12.3}\,h^{-1}\,M_\odot$ at $z = 0.4$ and that the halo radius for M_{B_*} galaxies is $R_{200} = 212\,h^{-1}$ physical kpc. The best-fit $R_{\rm gas*}$ from Equation (7) therefore implies $R_{\rm gas} \approx 0.4\,R_{200}$.

Next, we derive the expected scaling relation between $R_{\rm gas}$ and halo mass M_h. The halo occupation analysis of 2dFGRS galaxies from Tinker et al. (2007) showed that the relationship between M_h and luminosity for galaxies of $L_{b_J} \lesssim L_*$ at $z \sim 0.1$ is $M_h = 10^{12.5}(L_B/L_{B_*})^{1.3}\,h^{-1}\,M_\odot$. this monotonic relationship is appropriate for galaxies that reside at the *centers* of their dark matter halos and are the brightest galaxy in the halo. A similar scaling relation was obtained from DEEP2 data by ZCZ07 for galaxies at $z \sim 1$. Because there is a monotonic relationship between halo mass and galaxy luminosity, the scaling relation of $R_{\rm gas}$ with L_B in Equation (2) is equivalent to a scaling relation between M_h and R_{200} that are related by $M_h \propto R_{200}^3$. Adopting $\beta = 0.35$ from Equation (6), we derive $R_{\rm gas} = R_{\rm gas*} \times [M_h/(10^{12.3}\,h^{-1}\,M_\odot)]^{0.3}\,h^{-1}$ kpc at $z \sim 0.4$.

The calculations above show that observations support the initial assumptions in TC08 that the gaseous radius is a constant fraction of the halo radius for all halos and that the gaseous radius scales with halo mass according to M_h^t with $t \approx 1/3$. We note that our galaxy sample therefore probes halo mass range from $10^{10.5}\,h^{-1}\,M_\odot$ to $10^{12.8}\,h^{-1}\,M_\odot$, and that the best-fit scaling relation is driven by galaxies in the cold-hot transition regime. Next, we compare the observed covering fraction of Mg II absorbers with the predicted mean of TC08.

As summarized in § 1, we find in the halo occupation analysis of TC08 that dark matter halos of $M_h = 10^{11.5\text{–}12.5}\,h^{-1}\,M_\odot$ on average have a covering fraction of unity $\langle\kappa(M_h)\rangle = 1$ at $R_{\rm gas} \le R_{200}/3$ for Mg^+ and $\langle\kappa(M_h)\rangle = 0$ at larger radii. This halo mass range corresponds to a luminosity range of $L_B = 0.2 - 1.4\,L_{B_*}$ at $z \sim 0.4$, following the mass-to-light scaling relation discussed above. Sixteen galaxies in our sample have $L_B \ge 0.2\,L_{B_*}$, eleven of which are at $\log\rho + 0.14 \times (M_B - M_{B_*}) < \log R_{\rm gas*}$. We identify a corresponding Mg II absorber for every one of these galaxies, indicating a mean covering fraction of $\langle\kappa\rangle = 100$ % at $R < R_{\rm gas}$. This empirical result agrees with our model expectation. To assess the significance of detecting a Mg II absorber in every galaxy in the sample of eleven, we adopt the binomial distribution function and find that we can constrain the underlying mean covering factor at $\langle\kappa\rangle > 0.76$ with greater than 95% confidence level.

Three of the seven remaining $L_B < 0.2\,L_{B_*}$ galaxies in our sample have $\log\rho + 0.14 \times (M_B - M_{B_*}) < \log R_{\rm gas*}$. Two of them do not have corresponding Mg II absorbers identified to a sensitive upper limit, implying $\langle\kappa\rangle = 33$ % at $R < R_{\rm gas}$ for fainter galaxies (presumably lower-mass halos). This is also consistent with the expectation of TC08, where we found a quickly declining $\langle\kappa\rangle$ for halos of $M_h < 10^{11.5}\ h^{-1}\,M_\odot$, although the observations have a much lower statistical significance. In addition, we note that there exists an intrinsic scatter in the fiducial scaling relation between M_h and L_B. This intrinsic scatter is expected to smear out the exact edge of gaseous halos, particularly when considering an ensemble of objects with a wide range of luminosity.

In summary, the initial results from the on-going survey of Mg II absorbers in the vicinity of known galaxies close to QSO lines of sight have allowed us to study in detail the properties of extended gas around galaxies. The best-fit scaling relation between the extent of Mg^+ and galaxy luminosity and the observed mean gas covering fraction together provide strong empirical evidence to support the halo occupation model of TC08. To improve the statistical significances of various empirical parameters and to obtain a better understanding of the incidence of cold gas in dark matter halos, such as κ vs. M_h and κ vs. ρ, a larger sample of galaxy and Mg II absorber pairs established for a wide range of galaxy luminosity and morphology is necessary. In particular, only three galaxies in our current sample would be considered in a "cold-mode" halo based on their luminosity and none shows a corresponding Mg II absorber. Deep surveys targeting at fainter dwarfs are necessary to probe these "cold-mode" halos. Finally, we encourage observations of Mg II absorbers along the lines of sight toward close QSO pairs for obtaining a direct measure of the incidence of Mg^+ in individual halos.

We thank J.-R. Gauthier, J. O'Meara, M. Rauch and G. Becker for assistance on obtaining part of the MIKE spectra presented in this paper. We thank N. Gnedin and M. Rauch for helpful comments on an early version of the paper. This research has made use of the NASA/IPAC Extragalactic Database (NED) which is operated by the Jet Propulsion Laboratory, California Institute of Technology, under contract with the National Aeronautics and Space Administration. H.-W.C. acknowledges partial support from NASA Long Term Space Astrophysics grant NNG06GC36G and an NSF grant AST-0607510.

[10] We note that the fraction of satellite galaxies is $\lesssim 15$ % for L_* galaxies (Tinker et al. 2007; ZCZ07). In addition, none of the galaxies in our sample are observed to be part of a larger group or cluster. Here we carry out our calculations, assuming that most of galaxies in our sample are central galaxies in their dark matter halos.

REFERENCES

Bajtlik, S., Duncan, R. C., & Ostriker, J. P. 1988, 327, 570
Bechtold, J. & Ellingson, E. 1992, ApJ, 396, 20
Bergeron, J. 1986, A&A, 155, L8
Bergeron, J. & Stasínska, G. 1986, A&A, 169, 1
Bernstein, R. et al. 2003, Proc. SPIE, 4841, 1694, Shectman, S. A., Gunnels, S. M., Mochnacki, S., & Athey, A. E. 2003, Proc. SPIE, 4841, 1694
Birnboim, Y. & Dekel, A. 2003, MNRAS, 345, 349
Birnboim, Y., Dekel, A., & Neistein, E. 2007, MNRAS, 380, 339
Bond, N. A., Churchill, C. W., & Charlton, J. C. 2001, ApJ, 562, 641
Bowen, D. V., Blades, J. C., & Pettini, M. 1995, ApJ, 448, 634
Bouché, N., Murphy, M. T., & Péroux, C. 2004, MNRAS, 354, L25

Bouché, N., Murphy, M. T., Péroux, C., Csabai, I., & Wild, V. 2006, MNRAS, 371, 495
Cayatte, V., Kotanyi, C., Balkowski, C., & van Gorkom, J.H. 1994, AJ, 107, 1003
Chelouche, D., Ménard, B., Bowen, D. V., & Gnat, O. 2007, ApJ in press, (astro-ph/0706.4336)
Chen, H.-W. et al. 1998, ApJ, 498, 77, Lanzetta, K. M., Webb, J. K., & Barcons, X. 1998, ApJ, 498, 77
_____. 2001a, ApJ, 559, 654
Chen, H.-W., Lanzetta, K. M., & Webb, J. K. 2001b, ApJ, 556, 158
Churchill, C. W., Mellon, R. R., Charlton, J. C., Jannuzi, B. T., Kirhakos, S., Steidel, C. C., & Schneider, D. P. 2000, ApJS, 130, 91
Colless et al. 2001, MNRAS, 328, 1039
Davé, R., Hernquist, L., Katz, N., & Weinberg, D. H. 1999, ApJ, 511, 521
Dekel, A. & Birnboim, Y. 2006, MNRAS, 368, 2
D'Odorico, S., Cristiani, S., Dekker, H., et al. 2000, in SPIE 4005,Discoveries and Research Prospects from 8- to 10-Meter-Class Telescopes, ed. J. Bergeron, 121
Doherty, M., Bunker, A., Sharp, R., Dalton, G., Parry, I., & Lewis, I. 2006, MNRAS, 370, 331
Doyle, M. T. et al. 2005, MNRAS, 361, 34
Ellingson, E., Green, R. F., & Yee, H. K. C. 1991, ApJ, 378, 476
Faber, S. M. et al. 2007, ApJ, 665, 265
Ferland, G. J. et al. 1998, PASP, 110, 761
Guillemin, P. & Bergeron J. 1997, A&A, 328,, 499
Hamann, F. 1997, ApJS, 109, 279
Kacprzak, G. G., Churchill, C. W., Steidel, C. C., Murphy, M. T., & Evans, J. L. 2007, ApJ, 662, 909
Kereš, D., Katz, N., Weinberg, D. H., & Davé, R. 2005, MNRAS, 363, 2
Kravtsov, A. V. 2003, ApJ, 590, L1
Lanzetta, K. M. & Bowen, D. 1990, ApJ, 357, 321
Lanzetta, K. M., Bowen, D. V., Tytler, D., & Webb, J. K. 1995, ApJ, 442, 538
Maller, A. H. & Bullock, J. S. 2004, MNRAS, 355, 694
Mo, H. J. & Miralda-Escudé, J. 1996, ApJ, 469, 589
Mobasher, B. et al. 2004, ApJ, 600, L143
Navarro, J. F., Frenk, C. S., & White, S. D. M. 1996, ApJ, 490, 493
Nestor, D. B., Turnshek, D. A., & Rao, S. M. 2005, ApJ, 628, 637
Nestor, D. B., Turnshek, D. A., Rao, S. M., & Quider, A. M. 2007, ApJ, 658, 185
Petitjean, P. & Bergeron, J. 1990, A&A, 231, 309
Prochter, G. E., Prochaska, J. X., & Burles, S. M. 2006a, ApJ, 639, 766
Prochter, G. E., Prochaska, J. X., & Chen. H.-W. et al. 2006b, ApJ, 648, L93
Rao, S. M., Turnshek, D. A., & Nestor, D. B. 2006, ApJ, 636, 610
Rauch, M., Sargent, W. L. W., Barlow, T. A., & Simcoe, R. A. 2002, ApJ, 576, 45
Scott, J., Bechtold, J., Morita, M., Dobrzycki, A., & Kulkarni, V. P. 2002, ApJ, 571, 665
Steidel, C. C. 1995, in QSO Absorption Lines, Proceedings of the ESO Workshop Held at Garching, Germany, 21 - 24 November 1994, edited by Georges Meylan. Springer-Verlag Berlin Heidelberg New York. Also ESO Astrophysics Symposia, 1995., p.139, ed. G. Meylan, 139
Steidel, C. C., Dickinson, M., & Persson, S. E. 1994, ApJL, 437, L75
Steidel, C. C., Dickinson, M., Meyer, D. M., Adelberger, K. L., & Sembach, K. R., 1997, ApJ, 480, 568
Sternberg, A., McKee, C. F., & Wolfire, M. G. 2002, ApJS, 143, 419
Thilker, D. A. et al. 2004, ApJ, 601, L39
Tinker, J. L., Norberg, P., Weinberg, D. H., & Warren, M. S. 2007, ApJ, 659, 877
Tinker, J. L. & Chen, H.-W. 2008, ApJ submitted (arXiv:0709.1470)
Tresse, L., Maddox, S. J.;, Le Fèvre, O., & Cuby, J.-G. 2002, MNRAS, 337, 396
Tripp, T. M. & Bowen, D. V. 2005, in IAU Colloq. 199: Probing Galaxies through Quasar Absorption Lines, ed. P. Williams, C.-G. Shu, & B. Menard, 5–23
van den Bosch, F. C., Yang, X., Mo, H. J., Weinmann, S. M., Macciò, A. V., More, S., Cacciato, M., Skibba, R., & Kang, X. 2007, MNRAS, 376, 841
Veilleux, C., Cecil, G., & Bland-Hawthorn, J. 2005, ARA&A, 43, 769
Wang, B. 1993, ApJ, 415, 174
Wolfe, A. M., Gawiser, E., & Prochaska, J. X. 2005, ARA&A, 43, 861
Zheng, Z., Coil, A. L., & Zehavi, I. 2007, ApJ, 667, 760 (ZCZ07)
Zibetti, S., Ménard, B., Nestor, D., & Turnshek, D. 2005, ApJL, 631, L105